sustainability

MDPI

Article

Climate Data to Predict Geometry of Cracks in Expansive Soils in a Tropical Semiarid Region

Jacques Carvalho Ribeiro Filho [1], Eunice Maia de Andrade [2], Maria Simas Guerreiro [3,*], Helba Araujo de Queiroz Palácio [4] and José Bandeira Brasil [1]

[1] Departamento de Engenharia Agrícola, Campus do Pici, Universidade Federal do Ceará, Fortaleza 60455-760, CE, Brazil; jacquesfilho@alu.ufc.br (J.C.R.F.); josebandeira@alu.ufc.br (J.B.B.)
[2] Departamento de Conservação de Solo e Água, Universidade Federal Rural do Semi-Árido, Rua Francisco Mota, 572, Mossoró 59625-900, CE, Brazil; eunice.andrade@ufersa.edu.br
[3] FP-ENAS, Universidade Fernando Pessoa, Praça 9 Abril, 4249-004 Porto, Portugal
[4] Instituto Federal de Educação, Ciência e Tecnologia do Ceará, Rodovia Iguatu-Várzea Alegre, km 5, Iguatu 63503-790, CE, Brazil; helbaraujo@ifce.edu.br
* Correspondence: mariajoao@ufp.edu.pt

Abstract: The nonlinear dynamics of the determining factors of the morphometric characteristics of cracks in expansive soils make their typification a challenge, especially under field conditions. To overcome this difficulty, we used artificial neural networks to estimate crack characteristics in a Vertisol under field conditions. From July 2019 to June 2020, the morphometric characteristics of soil cracks (area, depth and volume), and environmental factors (soil moisture, rainfall, potential evapotranspiration and water balance) were monitored and evaluated in six experimental plots in a tropical semiarid region. Sixty-six events were measured in each plot to calibrate and validate two sets of inputs in the multilayer neural network model. One set was comprised of environmental factors with significant correlations with the morphometric characteristics of cracks in the soil. The other included only those with a significant high and very high correlation, reducing the number of variables by 35%. The set with the significant high and very high correlations showed greater accuracy in predicting crack characteristics, implying that it is preferable to have fewer variables with a higher correlation than to have more variables of lower correlation in the model. Both sets of data showed a good performance in predicting area and depth of cracks in the soils with a clay content above 30%. The highest dispersion of modeled over predicted values for all morphometric characteristics was in soils with a sand content above 40%. The model was successful in evaluating crack characteristics from environmental factors within its limitations and may support decisions on watershed management in view of climate-change scenarios.

Keywords: artificial intelligence; swelling and shrinking; Vertisol; tropical dry regions

Citation: Ribeiro Filho, J.C.; de Andrade, E.M.; Guerreiro, M.S.; de Queiroz Palácio, H.A.; Brasil, J.B. Climate Data to Predict Geometry of Cracks in Expansive Soils in a Tropical Semiarid Region. *Sustainability* **2022**, *14*, 675. https://doi.org/10.3390/su14020675

Academic Editor: Georgios Koubouris

Received: 18 December 2021
Accepted: 4 January 2022
Published: 8 January 2022

1. Introduction

Soil cracking is a natural phenomenon observed in soils with expansive clay minerals upon desiccation, and occurs mostly in drylands that cover approximately 40% of the world's land area [1] in South Africa, Australia, America, India, and China. Vertisols cover approximately 335 Mha [2], and are more common in the semiarid tropics [2,3] with an annual rainfall between 500 mm and 1000 mm, expanding when wet and contracting when dry, due to the high content of the expansive 2:1 clay mineral. The swelling and shrinking nature of expansive vertic soils may damage civil engineering structures [4,5], promote environmental pollution through preferential flow paths and compromise carbon storage [6], compromise tilling in agricultural fields [7,8], and affect slope stability [3,9].

Even though there is relevant information available [3,10], understanding the expansion and contraction processes in expansive soils at the field scale still remains a challenge

to optimize their use and management [3,10–12]. Field studies on the cracks–soil–water–environment interaction are scarce [3,10] when compared with laboratory studies [3].

Because of the scarcity of data on the morphometric characteristics of soil cracks at most locations, there is a need to develop models to be applied at locations with monitoring limitations. These models should rely on input variables obtained at lower costs in relation to traditional collection methods. Artificial intelligence has been successfully applied in the field of water resource management [13,14], and in recent years models based on artificial neural networks (ANN) have attracted researchers to the study of water–soil–environment interactions.

Prediction models using artificial neural networks need less calibration and validation data than traditional models. Thus, the technique is more economical and easier to use while maintaining the accuracy of the results. This research aims to develop and apply an artificial neural network model based on climate variables to estimate the morphometric parameters of cracks formed under field conditions in a semiarid environment.

2. Materials and Methods

2.1. Study Area

The study was developed in a catchment representative of a seasonally dry tropical forest in a semiarid environment. The historical mean annual rainfall of the region is 997 ± 300 mm, of which 89% is concentrated in the period from December to May [15]. The average potential evaporation is 2113 mm year^{-1}, with an aridity index of 0.48 [16].

The 2.8 ha first-order catchment study area is under regeneration after deforestation, burning and planting of pasture in 2010 in northeastern Brazil. Six (1 m × 1 m) plots (P1–P6) were randomly placed in the soft relief catchment to monitor crack characteristics (Figure 1). The plots were visited every week, with additional visits after a rainfall event.

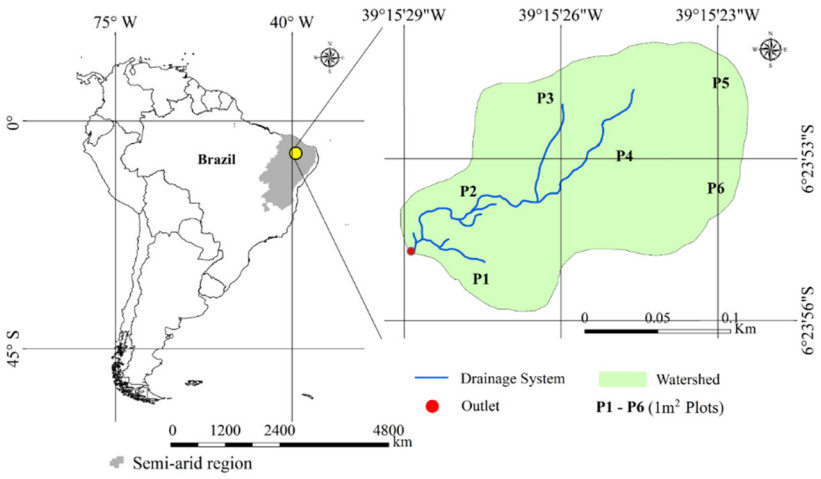

Figure 1. Catchment location.

The catchment soil is classified as a Vertisol [17], with a predominance of expansive 2:1 clay minerals of the montmorillonite group. The soil characteristics of each plot are presented in Table 1.

Table 1. Soil properties.

Soil Properties	Observed Plots					
	P1	**P2**	**P3**	**P4**	**P5**	**P6**
Grain size analysis						
Sand (%)	21	26	41	22	27	44
Silt (%)	43	46	33	41	41	36
Clay (%)	36	28	26	37	32	20
Organic matter (%)	0.8	1.5	1.3	1.4	1.9	2.2
Base saturation (%)	92	95	84	95	92	89
pH	6.6	7.1	6	6.8	6.6	6.7
Specific gravity	2.79	2.57	2.53	2.53	2.48	2.52
Liquid limit (%)	43	38	28	42	40	33
Plastic limit (%)	14	27	21	32	26	27
Plasticity index	30	12	7	10	14	7
Textural Classification	Clay loam	Clay loam	Sandy clay loam	Clay loam	Clay loam	Sandy clay loam

2.2. Data Acquisition

From July 2019 to June 2020, the morphometric characteristics of soil cracks (area, depth and volume), and environmental factors (soil moisture, rainfall, potential evapotranspiration and water balance) were monitored and evaluated in the six experimental plots. All readings were taken weekly and after a rainfall event, which totaled 65 days. A (0.05 m × 0.05 m) grid was permanently mounted at each (1 m × 1 m) plot with yellow plastic tape to follow the crack development (Figure 2b).

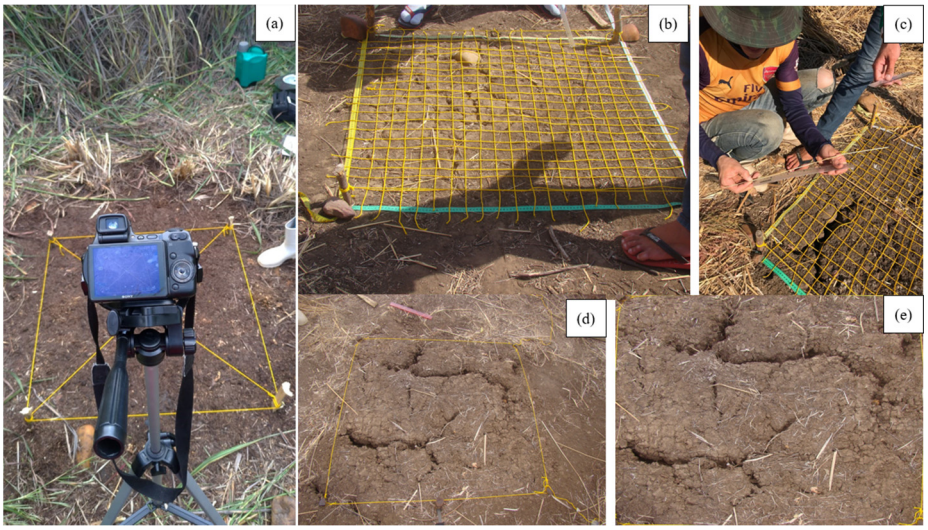

Figure 2. (**a**) Camera positioning for image collection; (**b**) grid with equidistant points for depth readings; (**c**) rod to read depth of cracks; (**d**) photographic image without correction for the horizontal; (**e**) image corrected for the horizontal plane.

During the monitoring visits, we took photographic images from each plot (Figure 2a). The camera was installed at 1 m height and at an angle of 30° relative to the experimental plot. All images were recorded with the same camera configuration—best shooting function, without zoom and with constant focus area [18]. The photographic images were corrected for a horizontal plane (Figure 2d,e) using the software GNU Image Manipulation Program (GIMP) version 2.10.10 (Available in: https://www.gimp.org/ accessed on 13 July 2020).

There were 390 selected images (65 days × 6 plots) based on technical criteria (shadow luminosity). After correction and selection, the images were analyzed for crack detection and the crack characteristics evaluated with the Software Crack Image Analysis System (CIAS) (Available in: http://acei.cn/program/CIAS/ accessed on 24 July 2020), iteratively.

After image digital processing and topological transformation, automatic quantification of the cracks' geometric characteristics (length, perimeter and area) was assessed as proposed by Liu et al. [19].

Based on the (0.05 m × 0.05 m) grid setup for each plot (Figure 2b) and a metric scale, we identified and measured crack characteristics (Figure 2c)–location, length, width and depth (Figure 2b,c). The measurements were taken with the aid of a caliper, a ruler, small vegetable rods and a laser distance meter. The volume of the cracks was evaluated assuming a parallelepiped form [20], being the product of the area of the crack by its depth (data available as Supplementary Materials).

Soil moisture content (SM) was determined daily, next to each plot, using the thermo-gravimetric method at a depth of 0.0–0.1m. Daily rainfall (PPT) was measured with a Ville de Paris rain gauge located at the outlet of the watershed, and potential evapotranspiration (PET) evaluated by the Hargreaves and Samani method [21] with calibrated parameters for the study area [22]. A simple water balance (WB) based on PPT and PET was evaluated daily (WB = PPT − PET).

2.3. Artificial Neural Network

To predict the morphometric characteristics of cracks in the soil based on climate and environmental data, we developed artificial neural network (ANN) models with the acquired data. We applied a Pearson correlation ($p < 0.05$) (Appendix A) between the input climatic variables and the output of cracks in the soil (Table 2).

Table 2. Input and output variables for the ANN model.

Input Environmental Variables	Output Cracks' Morphometric Characteristics Variables
• SM–daily soil moisture (%); • PPT01–PPT10–accumulated precipitation from previous 1 to 10 days (mm); • ET01–ET10–total potential evapotranspiration from previous 1 to 10 days (mm) • WB01–WB10–mean simplified water balance (mm)	• Depth • Area • Volume

Two models were developed:

- Model I—this model included all variables with a significant correlation ($p < 0.05$) (Appendix A), which were SM, PPT01-PPT10, ET01-ET10, WB01-WB10
- Model II—this model included the variables with a high or very high Pearson coefficient ($0.6 \leq |r| < 0.8$ or $0.8 \leq |r| < 1$, respectively), as suggested by Bisquerra et al. [23] with a significant correlation ($p < 0.05$), which were SM, ET01-ET10 (Appendix A).

We have developed multi-layer perceptron models, commonly applied in hydro environmental studies [24], which have a three-layer structure: the input layer, output layer and hidden layer (Figure 3). We used the hyperbolic tangent to activate the hidden layer and the identity function to activate the output layer, and we included a bias [14].

The models were trained and tested with different parts of the dataset (cross-validation). The choice of the data to be included in each sub-datasets (training and testing) was made so that each included all domains of the variables and contained the extreme values for calibration in order to be representative of all the available sample space.

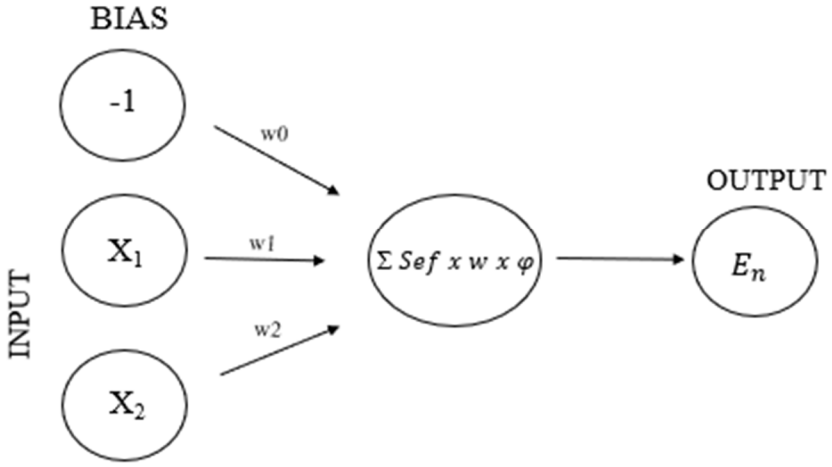

Figure 3. ANN multi-layer layout.

2.4. Model Performance

To analyze model performance, we compared the estimated to the observed results with coefficients that measure the average tendency of the simulated values to be larger or smaller than their observed ones: Nash–Sutcliffe (NS) coefficient [25] as suggested by Teixeira et al. [13] and Moriasi et al. [26], and percentage bias (PBIAS) [27] according to Moriasi et al. [26]: NS > 0.8 and PBIAS < 10—Excellent; 0.70 < NS $\leq$ 0.8 and 10 $\leq$ PBIAS < 15—Good; 0.45 < NS $\leq$ 0.7 and 15 $\leq$ PBIAS 20—Satisfactory; and NS $\leq$ 0.45 and PBIAS $\leq$ 20—Poor.

3. Results and Discussions

3.1. Spatial and Temporal Variability of Cracks' Morphometric Characteristics

The morphometric characteristics of soil cracks (area, depth and volume) (Figure 4) expressed variability over the period studied. The variability was associated with climatic seasonality. Over the dry period there was shrinking of the clays and forming of cracks, whereas when the rainy season began the clays expanded and the cracks were sealed [11]. Plots P1, P4 and P5 recorded the highest means for depths, area and volume of cracks, as well as the greatest variability.

During the study period all cracks sealed superficially at some point (Figure 4), and a value of zero was attributed to the variables of area, depth and volume. The highest values of area, depth and volume were recorded in Plot P1, which is closer to outlet (Figure 1). Although Plot P1 did not have the highest clay content, it had the highest limit of plasticity, which directly influenced the expansion/contraction process, both in the magnitude of occurrence and in the speed of the processes [4,28] when compared with the other plots.

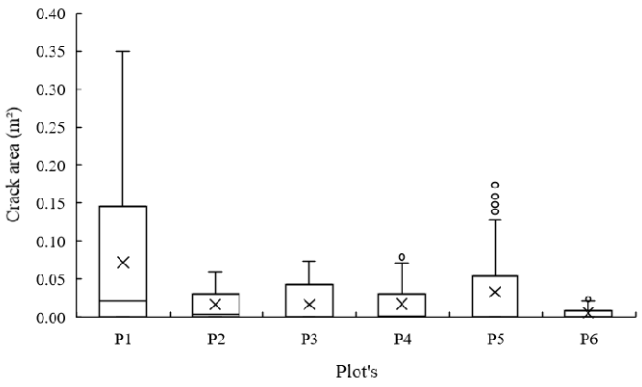

Figure 4. *Cont.*

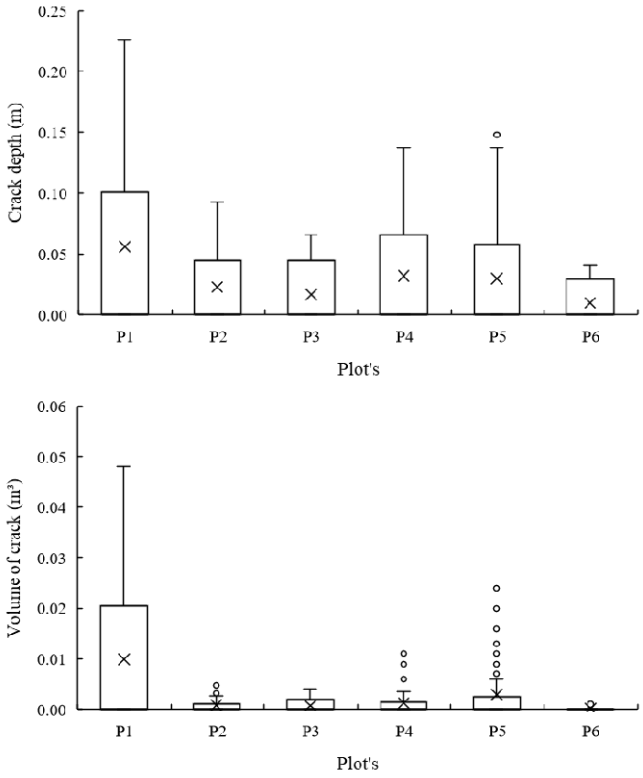

Figure 4. Morphometric descriptive characteristics of cracks in the Vertisol studied: area, depth and volume (× represent the median values and ° represent the outliers).

3.2. Models Performance

In determining the depth of cracks in the soil, Model II showed an excellent performance in both calibration and validation for all plots (Table 3), according to the classification criteria from Mosiari et al. [26]. Model I also showed an excellent performance for Plots P1, P2, P4 and P5 and satisfactory performance for Plots P3 and P6 on both calibration and validation. The lower clay content in Plots P3 and P6 (Table 1) reduced the degree of self-healing, being at that time governed by soil plasticity, which determines the potential for soil swelling and shrinking [28] directly, with a greater impact on Model I performance.

Model I showed a better performance (excellent) than Model II (good) for the variable area (Table 3) in Plots P1 and P5, and a satisfactory performance for the other plots, which showed an excellent performance in Model I and good performance when using Model I.

Still in Table 3, we observed that for the variable area in Plots P1 and P5, Model II presented performance classified as excellent according to Moriasi et al. [26], whereas Model I showed a good performance. For the other plots, both models displayed satisfactory performances. Plots P1 and P5 developed the largest crack areas (Figure 4), increasing the soil–crack connectivity [12] and interactions with external factors, leading to a higher performance of the models.

Of all soil crack morphometric characteristics (depth, area and volume) estimated by the two models (Table 3), the volume of cracks in Plot P6 was the only characteristic that in both models showed poor performance. For the other plots, the two models showed a satisfactory performance. Plot P6 had higher sand and lower clay contents and smaller crack areas, depths and volumes, revealing a smaller crack network which may have influenced the accuracy of the models [29].

Table 3. Model performance for determination of morphometric characteristics.

Depth of Cracks					
Plot	**Models**	**NS**		**PBIAS**	
		Calibration	**Validation**	**Calibration**	**Validation**
P1	Model I	0.94	0.91	0.62	0.97
	Model II	0.96	0.98	0.40	0.28
P2	Model I	0.70	0.77	1.29	0.88
	Model II	0.92	1.86	0.34	0.51
P3	Model I	0.73	0.57	0.82	0.66
	Model II	0.86	0.82	0.45	0.51
P4	Model I	0.88	0.88	0.68	0.79
	Model II	0.93	0.94	0.40	0.4
P5	Model I	0.82	0.83	1.22	0.84
	Model II	0.83	0.84	1.2	1.19
P6	Model I	0.65	0.55	0.56	0.66
	Model II	0.75	0.76	0.80	0.77
Area of Cracks					
Plot	**Models**	**NS**		**PBIAS**	
		Calibration	**Validation**	**Calibration**	**Validation**
P1	Model I	0.80	0.79	2.36	2.42
	Model II	0.83	0.82	2.03	2.07
P2	Model I	0.70	0.47	0.44	1.92
	Model II	0.80	0.69	0.90	1.09
P3	Model I	0.68	0.52	1.01	1.30
	Model II	0.84	0.82	0.49	0.50
P4	Model I	0.82	0.68	0.53	2.45
	Model II	0.71	0.46	0.87	2.18
P5	Model I	0.95	0.83	0.35	1.29
	Model II	0.95	0.83	0.35	1.26
P6	Model I	0.66	0.52	0.38	1.47
	Model II	0.65	0.46	0.38	1.5
Volume of Cracks					
Plot	**Models**	**NS**		**PBIAS**	
		Calibration	**Validation**	**Calibração**	**Validação**
P1	Model I	0.82	0.86	0.44	0.88
	Model II	0.8	0.64	0.47	0.28
P2	Model I	0.74	0.62	0.07	0.09
	Model II	0.88	0.87	0.03	0.03
P3	Model I	0.63	0.69	0.07	0.05
	Model II	0.80	0.82	0.04	0.03
P4	Model I	0.85	0.92	0.07	0.04
	Model II	0.82	0.86	0.04	0.02
P5	Model I	0.81	0.84	0.1	0.06
	Model II	0.86	0.94	0.16	0.06
P6	Model I	0,38	0.32	0.09	0.04
	Model II	0.42	0.36	0.08	0.04

3.3. Morphometric Characteristics of Soil Cracks

Both models predicted crack depth more accurately than the other variables at all plots (P1–P6), as may be observed in (Figures 5–10). Even though the models showed a satisfactory performance on the plots with higher sand contents (P3 and P6 in Table 1), there was high dispersion of the data when comparing the models' outputs with the observed data.

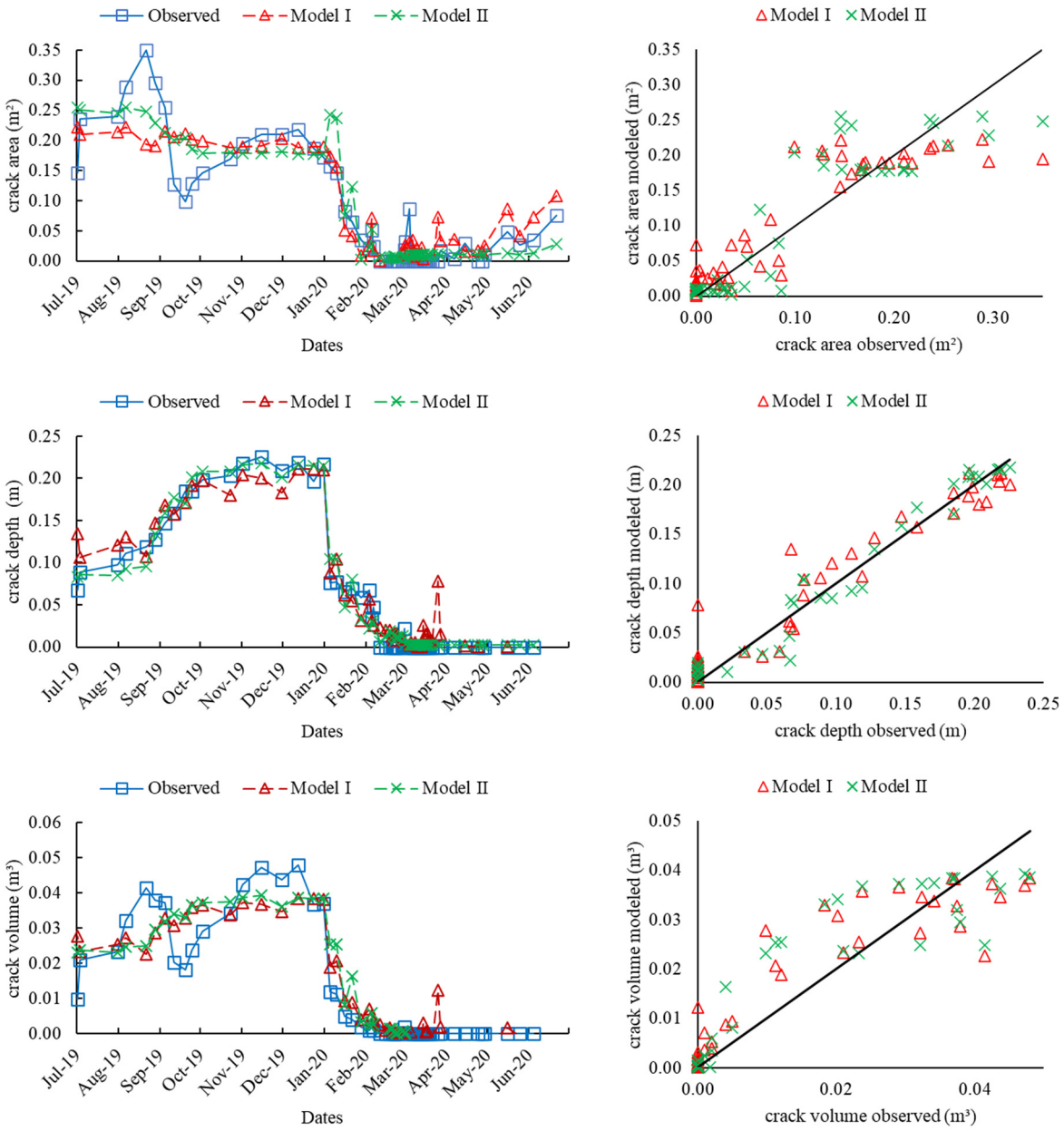

Figure 5. Morphometric characteristics of cracks in Plot P1: area, depth and volume (observed and modeled).

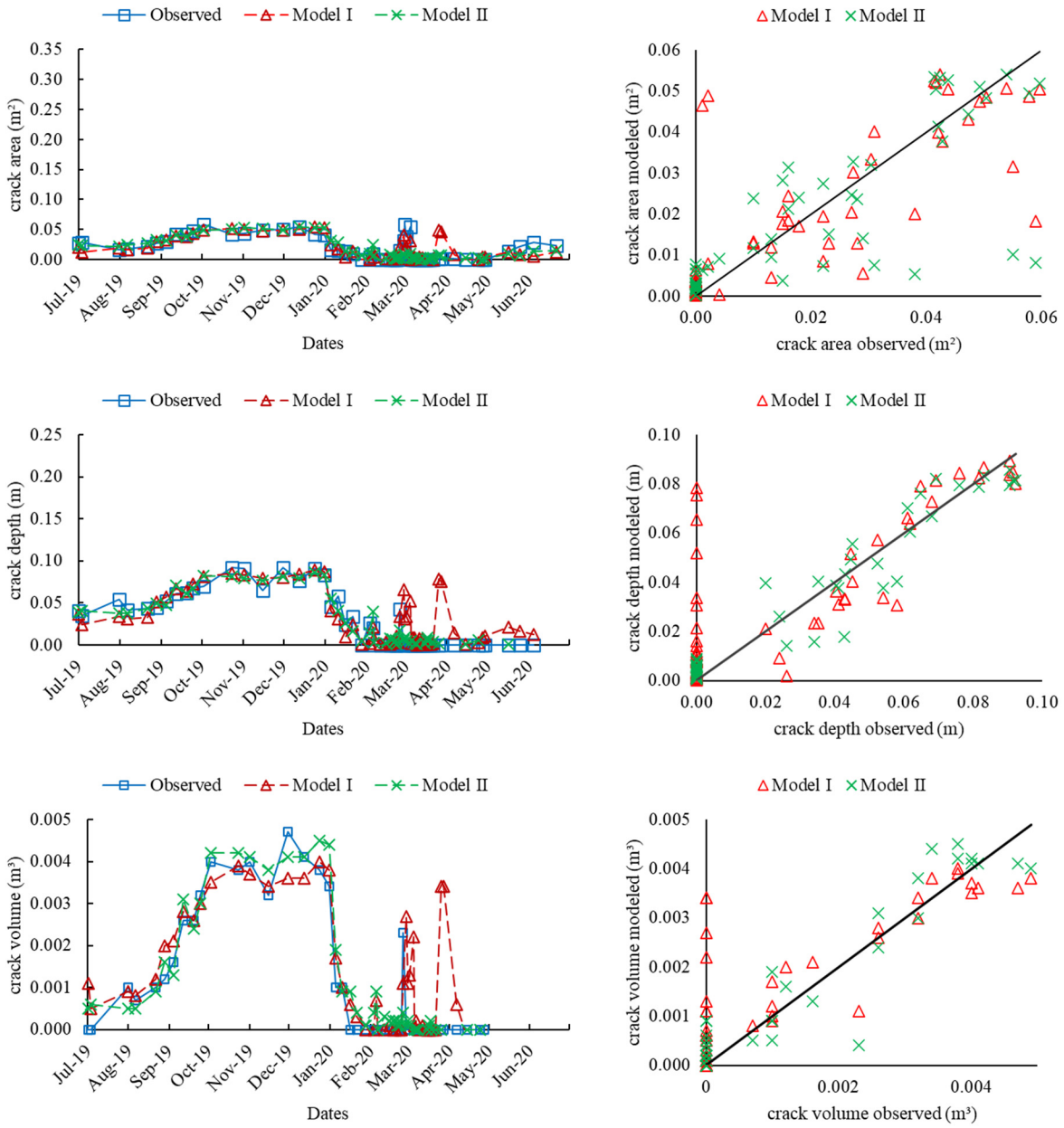

Figure 6. Morphometric characteristics of cracks in Plot P2: area, depth and volume (observed and modeled).

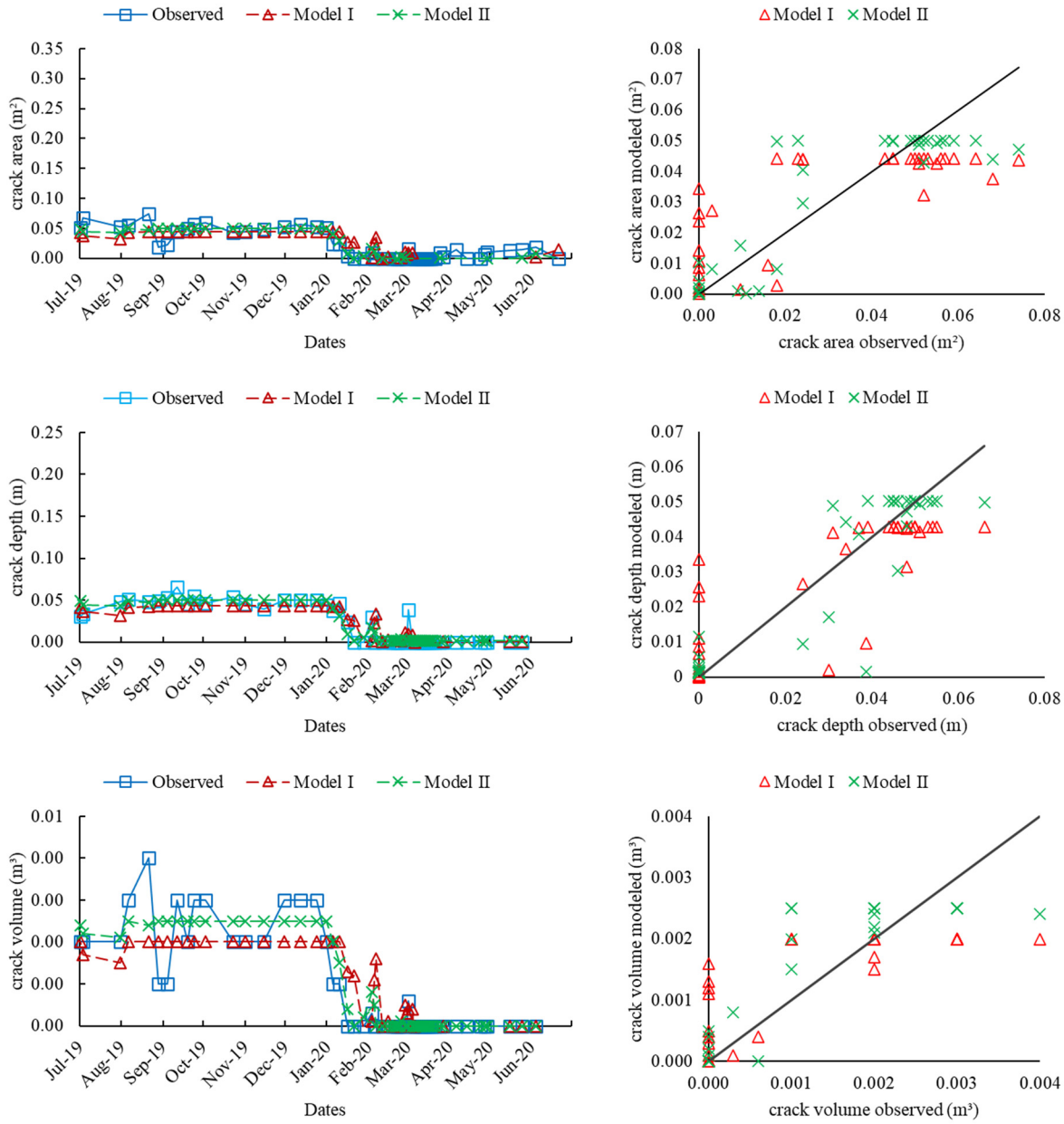

Figure 7. Morphometric characteristics of cracks in Plot P3: area, depth and volume (observed and modeled).

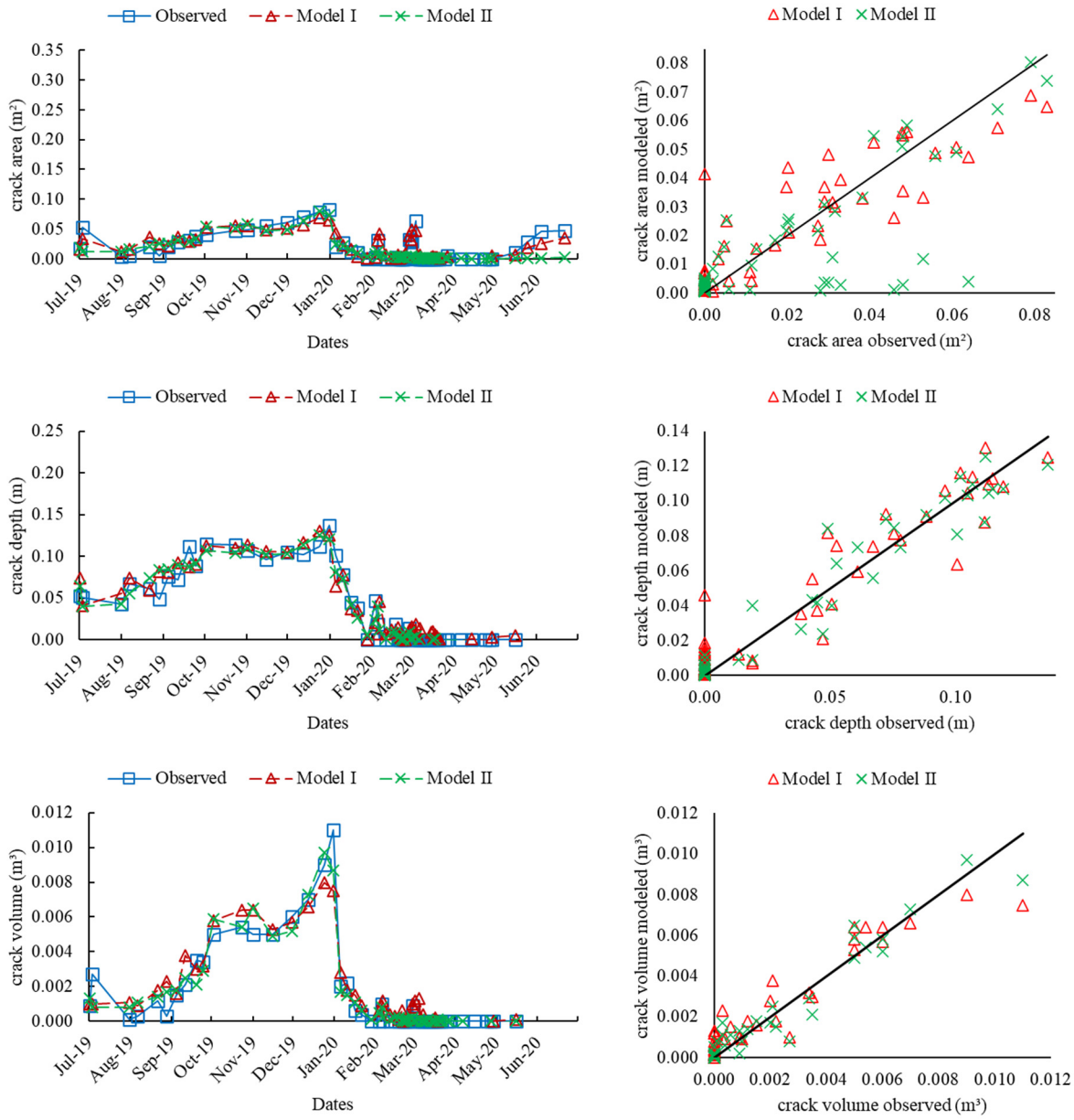

Figure 8. Morphometric characteristics of cracks in Plot P4: area, depth and volume (observed and modeled).

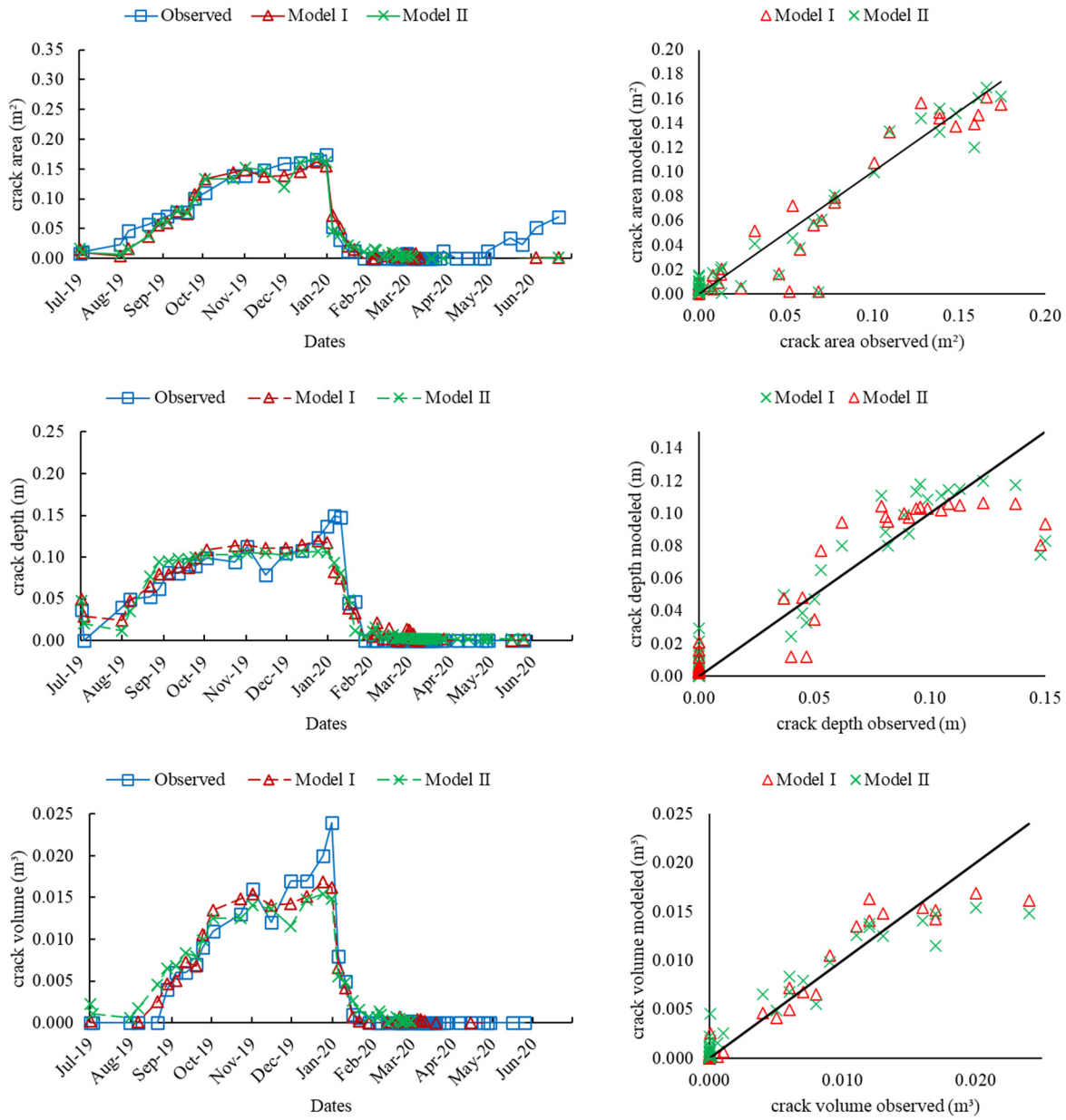

Figure 9. Morphometric characteristics of cracks in Plot P5: area, depth and volume (observed and modeled).

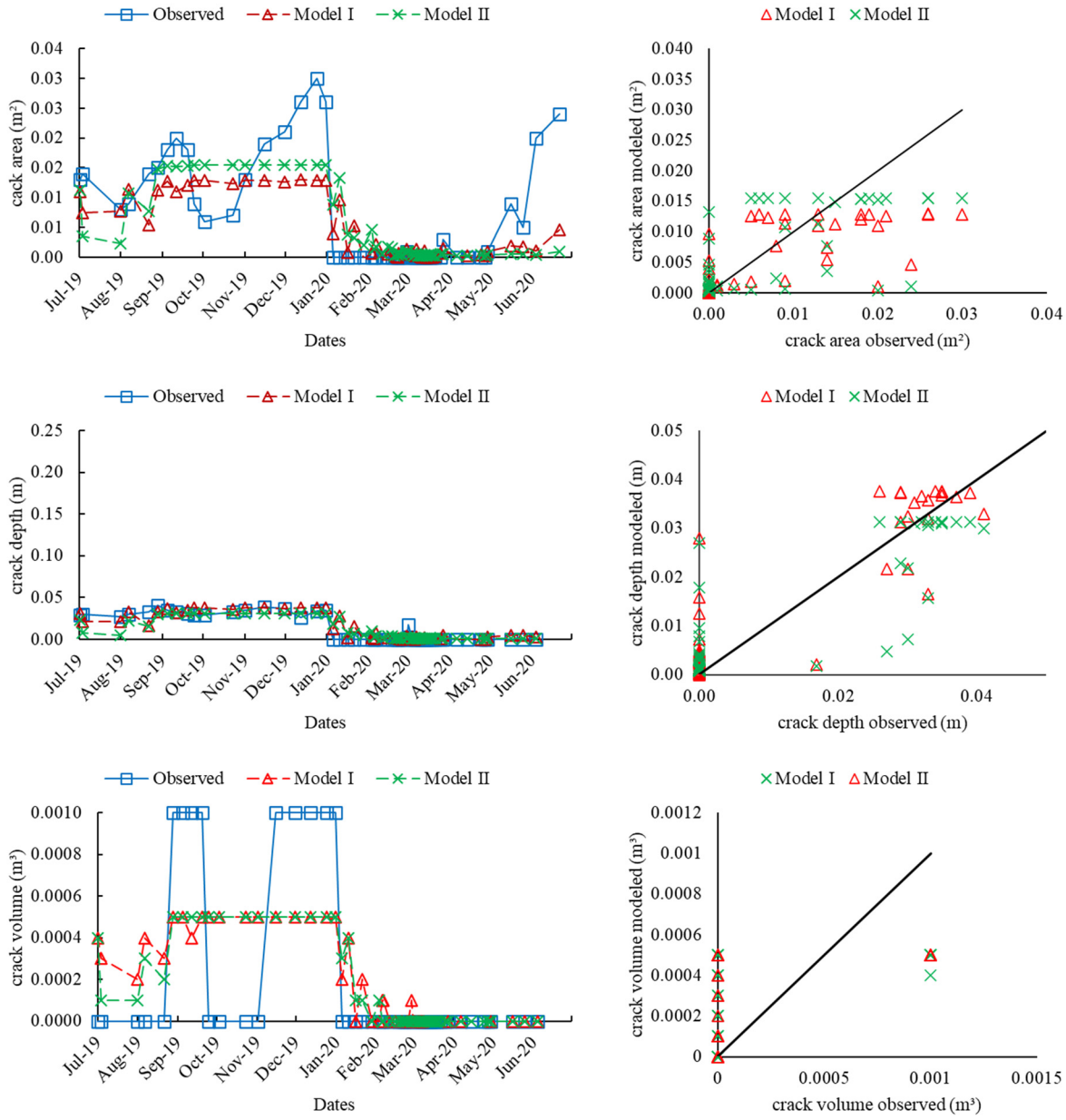

Figure 10. Morphometric characteristics of cracks in Plot P6: area, depth and volume (observed and modeled).

The estimates of the area of the cracks in the plots studied (Figures 5–10) with both models showed lower dispersions than were observed in the field in Plots P1 and P5, which had the highest plasticity indexes. The swelling/shrinking processes can occur quickly in clay with a high plasticity index [4,28]; hence, a faster response to climate variations can also occur. The higher sand content in Plots P3 and P6 decreased water adsorption when compared to soils with higher clay content [5], decreasing the cohesion forces [28], with consequent distinct responses to climatic conditions when compared to plots with higher clay contents (Figures 5–10). For the other plots (P2, P3, P4 and P6), there was greater dispersion of the models' outputs when compared to the observed values. It is also noted that in Plot P4, Model II underestimated the observed values when compared to Model I output, suggesting an influence of clay content on model response.

The temporal evolution of cracks' behavior is followed by both models (Figures 5–10), except for Plot P6, for which both models did not follow what was observed in the field: the models estimate a constant volume, although there are variations observed in the field.

Due to the higher sand content in this plot, the soil surface was under a higher stress caused by evaporation and resulting reduced soil moisture. These processes have an influence on the infiltration capacity/infiltration rate, which will affect crack formation, orientation and distribution, as well as crack sealing [30,31].

4. Conclusions

The neural network models developed in this study, based on climatic data to predict the morphometric characteristics of cracks in an expansive clay soil, determined well the area and depth of cracks in plots with a clay content above 30%. The models performed best when the input climatic variables showed high or very high correlations with the morphometric characteristics of cracks in the soil. The highest dispersions of modeled relative to observed values for all morphometric cracks' characteristics (area, depth and volume) were in plots with higher sand contents (above 40%). The model is suitable to be applied in regions with heavier soils and of higher clay contents.

Supplementary Materials: The following supporting information can be downloaded at: https://www.mdpi.com/article/10.3390/su14020675/s1.

Author Contributions: All authors made a significant contribution to the final version of the manuscript. Conceptualization, M.S.G., E.M.d.A., J.C.R.F. and H.A.d.Q.P.; methodology, M.S.G., J.B.B. and J.C.R.F.; writing—original draft preparation, M.S.G., J.C.R.F., E.M.d.A. and H.A.d.Q.P.; writing—review and editing, all authors; supervision, M.S.G., J.C.R.F. and E.M.d.A.; project administration, E.M.d.A. All authors have read and agreed to the published version of the manuscript.

Funding: This work was supported by CNPq–Conselho Nacional de Desenvolvimento Científico e Tecnológico, Brazil [grant number 558135/2009-9].

Institutional Review Board Statement: Not applicable.

Informed Consent Statement: Not applicable.

Data Availability Statement: The following supporting information can be downloaded at Supplementary Materials.

Acknowledgments: This study was carried out with the support of the Coordenação de Aperfeiçoamento de Pessoal de Nível Superior–Brasil (CAPES), the Conselho Nacional de Desenvolvimento Científico e Tecnológico (CNPq) and the Fundação Cearense de Apoio ao Desenvolvimento Científico e Tecnológico.

Conflicts of Interest: The authors declare no conflict of interest.

Appendix A

Table A1. Correlation between external environmental characteristics and morphometric features of cracks.

Variables	Plot P1			Plot P2			Plot P3			Plot P4			Plot P5			Plot P6		
	Area	Depth	Vol	Area	Depth	Vol	Area	Depth	Vol	Area	Depth	Vol	Area	Depth	Vol	Area	Depth	Vol
SM	−0.89 **	−0.90 **	−0.87 **	−0.84 **	−0.89 **	−0.75 **	−0.85 **	−0.88 **	−0.83 **	−0.75 **	−0.88 **	−0.71 **	−0.77 **	−0.81 **	−0.69 **	−0.74 **	−0.82 **	−0.63 **
ET1	0.61 **	0.78 **	0.72 **	0.72 **	0.76 **	0.74 **	0.66 **	0.67 **	0.68 **	0.65 **	0.76 **	0.71 **	0.77 **	0.71 **	0.73 **	0.70 **	0.70 **	0.61 **
ET2	0.63 **	0.87 **	0.79 **	0.79 **	0.84 **	0.82 **	0.71 **	0.72 **	0.72 **	0.76 **	0.84 **	0.81 **	0.85 **	0.79 **	0.83 **	0.74 **	0.74 **	0.60 **
ET3	0.67 **	0.89 **	0.83 **	0.82 **	0.86 **	0.84 **	0.75 **	0.76 **	0.75 **	0.78 **	0.85 **	0.82 **	0.87 **	0.79 **	0.83 **	0.77 **	0.78 **	0.61 **
ET4	0.67 **	0.90 **	0.82 **	0.83 **	0.87 **	0.85 **	0.74 **	0.76 **	0.75 **	0.78 **	0.88 **	0.83 **	0.88 **	0.82 **	0.84 **	0.75 **	0.77 **	0.61 **
ET5	0.68 **	0.90 **	0.83 **	0.84 **	0.88 **	0.87 **	0.74 **	0.78 **	0.75 **	0.80 **	0.89 **	0.85 **	0.89 **	0.83 **	0.86 **	0.75 **	0.77 **	0.61 **
ET6	0.67 **	0.91 **	0.83 **	0.86 **	0.89 **	0.88 **	0.74 **	0.78 **	0.76 **	0.83 **	0.90 **	0.87 **	0.91 **	0.84 **	0.88 **	0.76 **	0.77 **	0.62 **
ET7	0.67 **	0.91 **	0.83 **	0.86 **	0.90 **	0.89 **	0.75 **	0.79 **	0.77 **	0.83 **	0.90 **	0.88 **	0.92 **	0.85 **	0.89 **	0.77 **	0.78 **	0.63 **
ET8	0.69 **	0.93 **	0.84 **	0.87 **	0.91 **	0.90 **	0.77 **	0.80 **	0.79 **	0.84 **	0.91 **	0.88 **	0.92 **	0.85 **	0.89 **	0.78 **	0.79 **	0.63 **
ET9	0.68 **	0.92 **	0.84 **	0.86 **	0.90 **	0.90 **	0.75 **	0.79 **	0.77 **	0.84 **	0.91 **	0.88 **	0.92 **	0.85 **	0.89 **	0.77 **	0.78 **	0.63 **
ET10	0.67 **	0.92 **	0.83 **	0.85 **	0.90 **	0.89 **	0.75 **	0.79 **	0.76 **	0.84 **	0.90 **	0.88 **	0.92 **	0.84 **	0.89 **	0.76 **	0.77 **	0.63 **
PPT1	−0.37 **	−0.35 **	−0.35 **	−0.39 **	−0.41 **	−0.33 **	−0.35 **	−0.38 **	−0.34 **	−0.33 **	−0.37 **	−0.29 **	−0.31 **	−0.34 **	−0.27*	−0.29 **	−0.34 **	−0.29 **
PPT2	−0.51 **	−0.48 **	−0.49 **	−0.52 **	−0.52 **	−0.45 **	−0.48 **	−0.50 **	−0.47 **	−0.45 **	−0.47 **	−0.39 **	−0.42 **	−0.44 **	−0.37 **	−0.40 **	−0.47 **	−0.29 **
PPT3	−0.56 **	−0.54 **	−0.54 **	−0.55 **	−0.57 **	−0.47 **	−0.52 **	−0.55 **	−0.50 **	−0.48 **	−0.51 **	−0.42 **	−0.45 **	−0.48 **	−0.40 **	−0.43 **	−0.51 **	−0.31 **
PPT4	−0.61 **	−0.59 **	−0.58 **	−0.58 **	−0.59 **	−0.51 **	−0.55 **	−0.59 **	−0.53 **	−0.50 **	−0.54 **	−0.45 **	−0.49 **	−0.51 **	−0.43 **	−0.46 **	−0.55 **	−0.34 **
PPT5	−0.63 **	−0.61 **	−0.59 **	−0.60 **	−0.61 **	−0.52 **	−0.57 **	−0.61 **	−0.55 **	−0.52 **	−0.56 **	−0.46 **	−0.50 **	−0.53 **	−0.44 **	−0.47 **	−0.55 **	−0.34 **

Table A1. *Cont.*

Variables	Plot P1			Plot P2			Plot P3			Plot P4			Plot P5			Plot P6		
	Area	Depth	Vol	Area	Depth	Vol	Area	Depth	Vol	Area	Depth	Vol	Area	Depth	Vol	Area	Depth	Vol
PPT6	−0.64 **	−0.62 **	−0.61 **	−0.61 **	−0.63 **	−0.53 **	−0.61 **	−0.65 **	−0.59 **	−0.54 **	−0.59 **	−0.48 **	−0.51 **	−0.55 **	−0.45 **	−0.50 **	−0.58 **	−0.36 **
PPT7	−0.65 **	−0.63 **	−0.62 **	−0.61 **	−0.63 **	−0.54 **	−0.62 **	−0.66 **	−0.61 **	−0.53 **	−0.60 **	−0.49 **	−0.53 **	−0.57 **	−0.47 **	−0.52 **	−0.60 **	−0.37 **
PPT8	−0.67 **	−0.65 **	−0.64 **	−0.61 **	−0.64 **	−0.54 **	−0.64 **	−0.68 **	−0.62 **	−0.54 **	−0.62 **	−0.50 **	−0.54 **	−0.58 **	−0.48 **	−0.53 **	−0.61 **	−0.38 **
PPT9	−0.68 **	−0.66 **	−0.65 **	−0.61 **	−0.64 **	−0.54 **	−0.65 **	−0.68 **	−0.63 **	−0.54 **	−0.62 **	−0.50 **	−0.55 **	−0.60 **	−0.49 **	−0.54 **	−0.62 **	−0.39 **
PPT10	−0.68 **	−0.67 **	−0.65 **	−0.61 **	−0.64 **	−0.54 **	−0.66 **	−0.69 **	−0.64 **	−0.55 **	−0.64 **	−0.51 **	−0.56 **	−0.61 **	−0.50 **	−0.56 **	−0.63 **	−0.40 **
WB1	−0.41 **	−0.40 **	−0.40 **	−0.44 **	−0.46 **	−0.38 **	−0.39 **	−0.43 **	−0.38 **	−0.38 **	−0.43 **	−0.34 **	−0.36 **	−0.39 **	−0.32 **	−0.34 **	−0.39 **	−0.25*
WB2	−0.55 **	−0.54 **	−0.55 **	−0.57 **	−0.59 **	−0.52 **	−0.53 **	−0.55 **	−0.52 **	−0.51 **	−0.53 **	−0.46 **	−0.49 **	−0.50 **	−0.44 **	−0.46 **	−0.53 **	−0.34 **
WB3	−0.61 **	−0.61 **	−0.60 **	−0.61 **	−0.63 **	−0.54 **	−0.57 **	−0.61 **	−0.56 **	−0.54 **	−0.58 **	−0.49 **	−0.53 **	−0.54 **	−0.47 **	−0.49 **	−0.58 **	−0.36 **
WB4	−0.65 **	−0.65 **	−0.64 **	−0.64 **	−0.66 **	−0.58 **	−0.60 **	−0.64 **	−0.59 **	−0.57 **	−0.61 **	−0.52 **	−0.56 **	−0.58 **	−0.50 **	−0.52 **	−0.60 **	−0.39 **
WB5	−0.67 **	−0.68 **	−0.65 **	−0.66 **	−0.68 **	−0.59 **	−0.62 **	−0.67 **	−0.61 **	−0.58 **	−0.63 **	−0.53 **	−0.57 **	−0.59 **	−0.51 **	−0.53 **	−0.61 **	−0.39 **
WB6	−0.68 **	−0.69 **	−0.66 **	−0.68 **	−0.70 **	−0.60 **	−0.66 **	−0.71 **	−0.64 **	−0.61 **	−0.66 **	−0.55 **	−0.59 **	−0.62 **	−0.53 **	−0.56 **	−0.64 **	−0.41 **
WB7	−0.69 **	−0.70 **	−0.68 **	−0.68 **	−0.70 **	−0.61 **	−0.68 **	−0.71 **	−0.66 **	−0.60 **	−0.68 **	−0.56 **	−0.61 **	−0.64 **	−0.55 **	−0.58 **	−0.66 **	−0.43 **
WB8	−0.71 **	−0.72 **	−0.70 **	−0.69 **	−0.71 **	−0.62 **	−0.69 **	−0.73 **	−0.68 **	−0.62 **	−0.70 **	−0.58 **	−0.63 **	−0.66 **	−0.56 **	−0.60 **	−0.68 **	−0.44 **
WB9	−0.72 **	−0.74 **	−0.71 **	−0.69 **	−0.72 **	−0.63 **	−0.70 **	−0.74 **	−0.69 **	−0.62 **	−0.70 **	−0.58 **	−0.64 **	−0.67 **	−0.57 **	−0.61 **	−0.68 **	−0.45 **
WB10	−0.72 **	−0.75 **	−0.72 **	−0.69 **	−0.73 **	−0.63 **	−0.71 **	−0.75 **	−0.70 **	−0.63 **	−0.72 **	−0.60 **	−0.66 **	−0.68 **	−0.58 **	−0.62 **	−0.69 **	−0.46 **

area (m^2); depth (m); vol, volume (m^3); SM, soil moisture (%); ET1-ET10, accumulated potential evapotranspiration from 1 to 10 days (mm day^{-1}); PPT1-PPT10, accumulated precipitation from 1 to 10 days (mm); WB1-WB10, simplified water balance accumulated from 1 to 10 days (mm); ** Significant values at the level of 5%.

References

1. USS Working Group WRB. World Reference Base for Soil Resources 2014, Update 2015. International Soil Classification System for Naming Soils and Creating Legends for Soil Maps. World Soil Resources Reports No. 106; FAO: Rome, Italy, 2015. Available online: https://https://publications.jrc.ec.europa.eu/repository/handle/JRC91947 (accessed on 12 November 2021).
2. UN. 2010–2020: UN Decade for Deserts and the Fight Against Desertification 2019. [WWW Document]. Available online: https://www.un.org/en/events/desertification_decade/whynow.shtml (accessed on 16 September 2021).
3. Tang, C.S.; Zhu, C.; Cheng, Q.; Zeng, H.; Xu, J.J.; Tian, B.G.; Shi, B. Desiccation cracking of soils: A review of investigation approaches, underlying mechanisms, and influencing factors. *Earth-Sci. Rev.* **2021**, *216*, 103586. [CrossRef]
4. Wang, C.; Zhang, Z.Y.; Qi, W.; Fan, S.M. Morphological approach to quantifying soil cracks: Application to dynamic crack patterns during wetting-drying cycles. *Soil Sci. Soc. Am. J.* **2018**, *82*, 757–771. [CrossRef]
5. Cheng, Q.; Tang, C.S.; Xu, D.; Zeng, H.; Shi, B. Water infiltration in a cracked soil considering effect of drying-wetting cycles. *J. Hydrol.* **2021**, *593*, 125640. [CrossRef]
6. Mohanty, M.; Sinha, N.K.; Somasundaram, J.; McDermid, S.S.; Patra, A.K.; Singh, M.; Chaudhari, S.K. Soil carbon sequestration potential in a Vertisol in central India-results from a 43-year long-term experiment and APSIM modeling. *Agric. Syst.* **2020**, *184*, 102906. [CrossRef]
7. Dupdal, R.; Naik, B.S.; Patil, S.L.; Ramesha, M.N. Water Harvesting-Farm Pond as Source of Income and Livelihood Security for Rainfed Farmers in Semi-Arid Vertisols of Karnataka: A Success Story. *Biot. Res. Today* **2021**, *3*, 938–940.
8. Qi, W.; Zhang, Z.Y.; Wang, C. Desiccation and cracking behaviour of clay loam subjected to different irrigation methods during wetting–drying cycles. *Eur. J. Soil Sci.* **2021**, *72*, 793–809. [CrossRef]
9. Guney, Y.; Sari, D.; Cetin, M.; Tuncan, M. Impact of cyclic wetting–drying on swelling behavior of lime-stabilized soil. *Build. Environ.* **2007**, *42*, 681–688. [CrossRef]
10. Bordoloi, S.; Ni, J.; Ng, C.W.W. Soil desiccation cracking and its characterization in vegetated soil: A perspective review. *Sci. Total Environ.* **2020**, *729*, 138760. [CrossRef] [PubMed]
11. Bullard, J.E.; Ockelford, A.; Strong, C.L.; Aubault, H. Impact of multi-day rainfall events on surface roughness and physical crusting of very fine soils. *Geoderma* **2018**, *313*, 181–192. [CrossRef]
12. Xiong, D.; Yan, D.; Long, Y.; Lu, X.; Han, J.; Han, X.; Shi, L. Simulation of morphological development of soil cracks in Yuanmou Dry-hot Valley region, Southwest China. *Chin. Geogr. Sci.* **2010**, *20*, 112–122. [CrossRef]
13. Teixeira, L.C.; Mariani, P.P.; Pedrollo, O.C.; dos Reis Castro, N.M.; Sari, V. Artificial Neural Network and Fuzzy Inference System Models for Forecasting Suspended Sediment and Turbidity in Basins at Different Scales. *Water Resour. Manag.* **2020**, *34*, 3709–3723. [CrossRef]
14. Sari, V.; Dos Reis Castro, N.M.; Pedrollo, O.C. Estimate of suspended sediment concentration from monitored data of turbidity and water level using artificial neural networks. *Water Resour. Manag.* **2017**, *31*, 4909–4923. [CrossRef]
15. Campos, D.A.; de Andrade, E.M. Tendência Sazonal de VariáVeis Climáticas em uma área do Domínio Fitogeográfico da Caatinga. Revista Agro@mbiente On-line, v. 15. 2021, pp. 1–10. Available online: file:///C:/Users/MDPI/AppData/Local/Temp/6833-26737-1-PB.pdf (accessed on 15 May 2021).

16. Guerreiro, M.S.; Andrade, E.M.D.; Palácio, H.A.D.Q.; Brasil, J.B. Enhancing Ecosystem Services to Minimize Impact of Climate Variability in a Dry Tropical Forest with Vertisols. *Hydrology* **2021**, *8*, 46. [CrossRef]
17. *Soil Survey Staff. Keys to Soil Taxonomy*, 11th ed.; Chapter 16; United States Department of Agriculture, Natural Resources Conservation Service, U.S. Government Printing Office: Washington, DC, USA, 2010; pp. 287–298.
18. Bauer, T.; Strauss, P. A rule-based image analysis approach for calculating residues and vegetation cover under field conditions. *Catena* **2014**, *113*, 363–369. [CrossRef]
19. Liu, C.; Tang, C.S.; Shi, B.; Suo, W.B. Automatic quantification of crack patterns by image processing. *Comput. Geosci.* **2013**, *57*, 77–80. [CrossRef]
20. Stewart, R.D.; Najm, M.R.A. Field measurements of soil cracks. *Soil Sci. Soc. Am. J. 2020 84*, 1462–1476. [CrossRef]
21. Hargreaves, G.H.; Samani, Z.A. Reference crop evapotranspiration from temperature. *Appl. Eng. Agric.* **1985**, *1*, 96–99. [CrossRef]
22. De Lima, J.C.D.; Arraes, F.D.D.; Oliveira, J.B.D.; Nascimento, F.A.L.D.; Macêdo, K.G.D. Parametrização da equação de Hargreaves e Samani para estimativa da evapotranspiração de referência no Estado do Ceará, Brasil. *Rev. Cienc. Agron.* **2016**, *47*, 447–454. [CrossRef]
23. Bisquerra, R.; Sarriera, J.C.; Martínez, F. *Introdução à Estatística: Enfoque Informático Com o Pacote Estatístico SPSS*; Artmed: Porto Alegre, Brazil, 2004; 254p.
24. Rumelhart, D.E.; Hinton, G.E.; Williams, R.J. Learning representations by back-propagating errors. *Nature* **1986**, *323*, 533–536. [CrossRef]
25. Nash, J.E.; Sutcliffe, J.V. River flow forecasting through conceptual models part I—A discussion of principles. *J. Hydrol.* **1970**, *10*, 282–290. [CrossRef]
26. Moriasi, D.N.; Gitau, M.W.; Pai, N.; Daggupati, P. Hydrologic and water quality models: Performance measures and evaluation criteria. *Trans. ASABE* **2015**, *58*, 1763–1785. [CrossRef]
27. Gupta, H.V.; Sorooshian, S.; Yapo, P.O. Status of automatic calibration for hydrologic models: Comparison with multilevel expert calibration. *J. Hydrol. Eng.* **1999**, *4*, 135–143. [CrossRef]
28. Rayhani, M.H.T.; Yanful, E.K.; Fakher, A. Physical modeling of desiccation cracking in plastic soils. *Eng. Geol.* **2008**, *97*, 25–31. [CrossRef]
29. Vogel, H.J.; Hoffmann, H.; Leopold, A.; Roth, K. Studies of crack dynamics in clay soil: II. A physically based model for crack formation. *Geoderma* **2005**, *125*, 213–223. [CrossRef]
30. Dinka, T.M.; Morgan, C.L.; McInnes, K.J.; Kishné, A.S.; Harmel, R.D. Shrink–swell behavior of soil across a Vertisol catena. *J. Hydrol.* **2013**, *476*, 352–359. [CrossRef]
31. Sadeghi, S.H.; Kheirfam, H.; Darki, B.Z. Controlling runoff generation and soil loss from field experimental plots through inoculating cyanobacteria. *J. Hydrol.* **2020**, *585*, 124814. [CrossRef]